


Magnetic anisotropy and low-field magnetic phase diagram of the quasi-two-dimensional ferromagnet $\text{Cr}_2\text{Ge}_2\text{Te}_6$

S. Selter,^{1,2,*} G. Bastien,¹ A. U. B. Wolter,¹ S. Aswartham,^{1,†} and B. Büchner^{1,2}

¹*Institute for Solid State Research, Leibniz IFW Dresden, Helmholtzstrasse 20, 01069 Dresden, Germany*

²*Institute of Solid State and Materials Physics, Technische Universität Dresden, 01062 Dresden, Germany*

 (Received 12 June 2019; revised manuscript received 22 November 2019; published 27 January 2020)

All known quasi-two-dimensional ferromagnets, such as ($X = \text{Br}, \text{I}$) or $\text{Cr}_2(\text{Ge}, \text{Si})_2\text{Te}_6$, exhibit a peculiar temperature dependence of the magnetization under small magnetic fields applied in the hard plane. Investigating the van der Waals layered $\text{Cr}_2\text{Ge}_2\text{Te}_6$ by magnetization and specific-heat measurements under magnetic fields, we report the temperature dependence of the effective magnetic anisotropy as a plausible explanation for this unusual behavior. Magnetic temperature-field phase diagrams were measured for magnetic fields applied along the magnetic easy axis and in the hard plane up to 30 kOe and 150 K to obtain a detailed understanding of the magnetization behavior in the low-field region and especially below the magnetic saturation fields. From these magnetic phase diagrams the temperature dependence of the effective magnetocrystalline anisotropy constant is extracted and compared to the corresponding theory, unique for $\text{Cr}_2\text{Ge}_2\text{Te}_6$ until now. Based on the thermal evolution of the effective magnetocrystalline anisotropy constant and the aforementioned magnetic phase diagrams, a qualitative scheme is developed explaining the changes of magnetization direction due to the influence of temperature, as well as strength and direction of external magnetic fields in $\text{Cr}_2\text{Ge}_2\text{Te}_6$. Structural and magnetic similarities to other quasi-two-dimensional ferromagnets may allow this scheme to be generalized for the whole class of materials.

DOI: [10.1103/PhysRevB.101.014440](https://doi.org/10.1103/PhysRevB.101.014440)

I. INTRODUCTION

Since the discovery of graphene in 2004 [1], two dimensional (2D) materials have been in the forefront of research both in fundamental as well as in applied science. This class of materials stands out due to electronic properties in combination with unique structural characteristics [2–6]. On one hand, when thinned down to the monolayer limit, significant changes in the physical properties have been observed [2,3,6,7]. On the other hand, some materials conserve their bulk properties down to the monolayer limit, enabling different applications and architectures [8–10]. Examples are ferromagnetic monolayers, which have a great potential for applications in the field of spintronics and data storage devices.

As observed in $\text{Cr}_2\text{Ge}_2\text{Te}_6$ [11] and in structurally related CrI_3 [12], evidence for ferromagnetism at least down to the bilayer could be seen by magneto-optical-Kerr-effect (MOKE) microscopy. The structural relation between $\text{Cr}_2\text{Ge}_2\text{Te}_6$ and CrI_3 is given by a shared honeycomb motif in the ab plane. For the isostructural compound $\text{Cr}_2\text{Si}_2\text{Te}_6$ monolayer ferromagnetism is theoretically predicted [13] but still lacks experimental confirmation. Furthermore, Kitaev interactions were recently discussed to realize the magnetic exchange mechanism in the monolayer of these compounds [14]. It is

also worth mentioning that VSe_2 , a diamagnet in bulk, shows ferromagnetic ordering when prepared as a monolayer [15].

While the discovery of robust ferromagnetism in the monolayer limit itself is without doubt stunning and attracted significant attention in the scientific community due to the potential impact it can have in future applications, the bulk magnetic state in these compounds is not well understood. For example, for all mentioned bulk ferromagnets, an anomaly in the form of a maximum of the magnetization just below the Curie temperature can be observed applying relatively low fields in the corresponding magnetic hard plane [16–18]. A relation between this anomaly and the magnetic anisotropy of these systems seems obvious considering the recognizable strength of the latter [19,20]. Indeed, it is not coincidental to find significant magnetic anisotropy in potential 2D magnets but rather a requirement for long-range order in a system with reduced dimensionality. The Mermin-Wagner theorem [21] states that in isotropic low-dimensional magnetic systems ($D \leq 2$) the magnonic density of states is gapless. Subsequently, spin waves are excited at all finite temperatures disturbing static long-range magnetic order. However, introducing anisotropies in 2D systems leads to the opening of a gap in the magnon density of states, thus allowing for static long-range magnetic order. Subsequently, finding a significant magnetic anisotropy in 2D magnetic candidate materials may be anticipated [22,23].

Nevertheless, until now the origin and nature of the aforementioned magnetic anomaly remains elusive. However, to entangle the physics behind the intriguing phenomenon of monolayer ferromagnetism, a reliable understanding of the

*s.selter@ifw-dresden.de

†s.aswartham@ifw-dresden.de

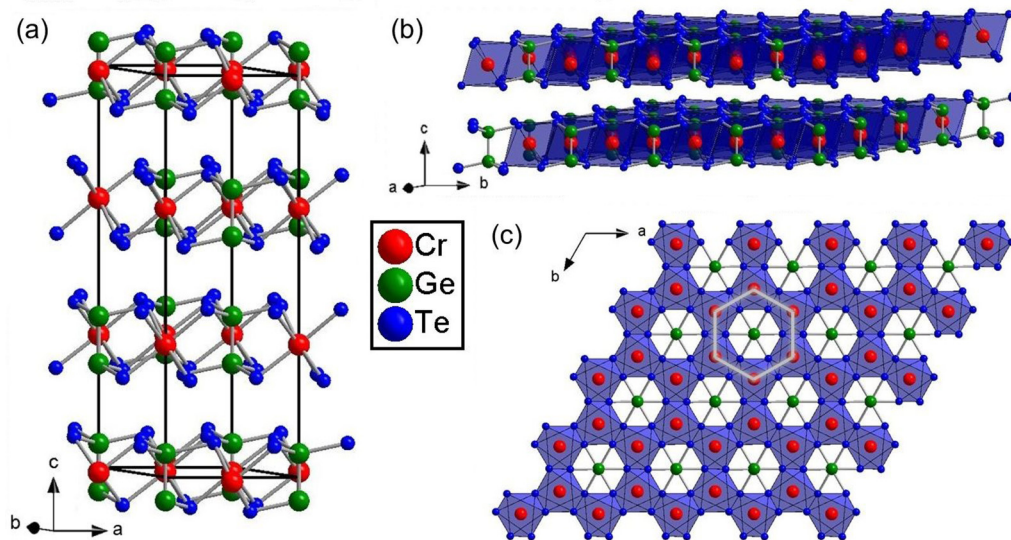


FIG. 1. Crystal structure of $\text{Cr}_2\text{Ge}_2\text{Te}_6$ in the space group $R\bar{3}$ (no. 148). (a) Unit cell of $\text{Cr}_2\text{Ge}_2\text{Te}_6$. (b) View perpendicular to the c axis showing the structural layers and their stacking. (c) View perpendicular to the ab plane showing the honeycomb network.

bulk magnetism and anisotropy is a prerequisite in these compounds.

$\text{Cr}_2\text{Ge}_2\text{Te}_6$ crystallizes in the trigonal space group $R\bar{3}$ (no. 148) and belongs to the class of layered van der Waals (vdW) transition metal trichalcogenides (TMTCs). This class of compounds possesses layers made of the respective transition metal (TM), octahedrally surrounded by the respective chalcogenide (C) [24,25]. Those edge-sharing TMC_6 octahedra form a honeycomb network. The void of each honeycomb is occupied by a dimer of a IV/V main group element (P, Si, Ge) with the binding axis between the two atoms perpendicular to the honeycomb plane. This dimer is a peculiarity which differentiates this structure from other honeycomb structures, such as CrX_3 ($X = \text{Cl}, \text{Br}, \text{I}$). As shown in Fig. 1(b), the honeycomb layers are stacked onto each other, well separated by a van der Waals (vdW) gap, which makes it easy to exfoliate crystals down to a few layers. The stacking of the layers varies in the family of TMTCs. For $\text{Cr}_2\text{Ge}_2\text{Te}_6$ and $\text{Cr}_2\text{Si}_2\text{Te}_6$ in the $R\bar{3}$ space group (no. 148), an ABC stacking is found. In contrast, $\text{Al}_2\text{Si}_2\text{Te}_6$ in the $P\bar{3}$ (no. 147) space group (with a main group metal instead of a transition metal) exhibits the highly ordered AAA stacking [26]. For the $\text{TM}_2\text{P}_2(\text{S}, \text{Se})_6$ family of compounds, the stacking is more difficult to generalize, since the stacking of the layers with respect to a perpendicular direction depends on the monoclinic β angle of the space group $C12/m1$ (no. 12) [27,28]. These considerations of the stacking do not explicitly take stacking faults into account.

TMTCs in general possess a nonzero band gap ranging from 0.5 to 3.5 eV mainly depending on the TM and the strong spin-orbit coupling together with electron correlations [29]. Furthermore, these compounds exhibit many different possibilities for long-range magnetic order, mainly depending on the TM ion. $\text{Cr}_2\text{Ge}_2\text{Te}_6$ in particular has a band gap of ~ 0.74 eV (direct) and ~ 0.2 eV (indirect) and a ferromagnetic ground state with the magnetic easy axis perpendicular to the layers [24,30]. This makes the title compound one of the rare examples of ferromagnetic semiconductors. Owing

to these properties and the nature of this class of materials to be easy to exfoliate, $\text{Cr}_2\text{Ge}_2\text{Te}_6$ found use as substrate for ferromagnetic insulator-topological insulator heterostructures [8]. Furthermore, the magnetic lattice of $\text{Cr}_2\text{Ge}_2\text{Te}_6$ (and also $\text{Cr}_2\text{Si}_2\text{Te}_6$) is the same as for CrX_3 ($X = \text{Br}, \text{I}$), since the Ge dimer in the void of the $\text{Cr}_2\text{Ge}_2\text{Te}_6$ honeycomb is magnetically inactive. Altogether, the known 2D vdW honeycomb ferromagnets exhibit an excellent platform to compare their magnetic interactions.

Here, we present a comprehensive experimental investigation of the anisotropic bulk magnetic properties of vdW-layered $\text{Cr}_2\text{Ge}_2\text{Te}_6$ single crystals by means of DC magnetometry and specific-heat measurements. We obtain the low-field magnetic phase diagram of this compound for the easy axis and hard plane, with the easy-axis being perpendicular to the honeycomb layers. Under magnetic fields applied parallel to the hard plane ab , a downturn with an onset temperature T^* is observed in the temperature-dependent magnetization curve. We explain this anisotropic and specific behavior for fields in the hard plane as an interplay among field, temperature, and effective magnetic anisotropy in $\text{Cr}_2\text{Ge}_2\text{Te}_6$.

II. SYNTHESIS, SAMPLE CHARACTERIZATION, AND METHODS

Single crystals of $\text{Cr}_2\text{Ge}_2\text{Te}_6$ with a size up to $6\text{mm} \times 5\text{mm} \times 0.2\text{mm}$ (see Fig. 2) were grown by the self-flux technique according to Zhang *et al.* [16]. Details regarding the growth procedure and an in-depth characterization of the crystals used in this work are published elsewhere [19]. Both powder x-ray diffraction and energy dispersive x-ray spectroscopy agree well with the published crystal structure in the $R\bar{3}$ space group [24] as well as with the expected stoichiometry of $\text{Cr}_2\text{Ge}_2\text{Te}_6$.

DC magnetization was measured as a function of temperature and field using a quantum interference device vibrating sample magnetometer (SQUID VSM) from Quantum Design. The values obtained for magnetic moments were corrected

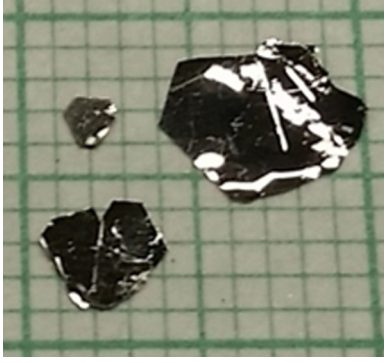


FIG. 2. As-grown crystals of $\text{Cr}_2\text{Ge}_2\text{Te}_6$ up to several mm size.

due to deviation of the measured sample shape and size from a point dipole. This correction follows the procedure described in Ref. [31]. A detailed description of how this correction is applied can be found in the Appendix of the work of Zeisner *et al.* [19].

Low-temperature specific heat was determined using a relaxation technique in a physical property measurement system (PPMS) from Quantum Design. The specific heat from the platform and grease used for mounting the sample were subtracted.

III. RESULTS AND DISCUSSION

A. Magnetic characterization

The zero-field specific heat of $\text{Cr}_2\text{Ge}_2\text{Te}_6$ divided by temperature C_p/T , and the temperature-dependent normalized magnetization M/H at 1 kOe applied parallel and perpendicular to the crystallographic ab plane as well as the inverse of the normalized magnetization are represented in Figs. 3(a)–3(c), respectively. For the normalized magnetization only the results from field-cooled measurements are shown since no significant difference of zero-field-cooled and field-cooled measurements was observed.

A Λ -shape peak in the temperature-dependent specific heat indicates a second-order phase transition at $T_C = 65$ K. In good agreement with this, a similar Curie temperature [$T_C = 66 (\pm 1)$ K] is obtained from the minimum of the first derivative of the temperature-dependent normalized magnetization for both crystallographic orientations. While no further phase transition was observed in the specific heat at zero field, the magnetization curves show an anomalous behavior for $H \parallel ab$ below T_C . A downturn towards lower T is observed below $T^* = 64$ K for $H \parallel ab$, whereas for $H \perp ab$ a typical ferromagnetic behavior is observed.

A similar anisotropic behavior is also seen for $\text{Cr}_2\text{Si}_2\text{Te}_6$ [32], CrI_3 [20], and CrBr_3 [20], which are also 2D honeycomb ferromagnets and which show a close relation to $\text{Cr}_2\text{Ge}_2\text{Te}_6$ regarding their structure. The similarities regarding structure, magnetic ion, and magnetic ordering hint towards a main role of these properties for the origin of the observed anisotropy.

At temperatures well above the Curie temperature in the paramagnetic state, a linear dependence between magnetization and field can be assumed. Therefore the magnetic susceptibility can be approximated by the normalized magnetization

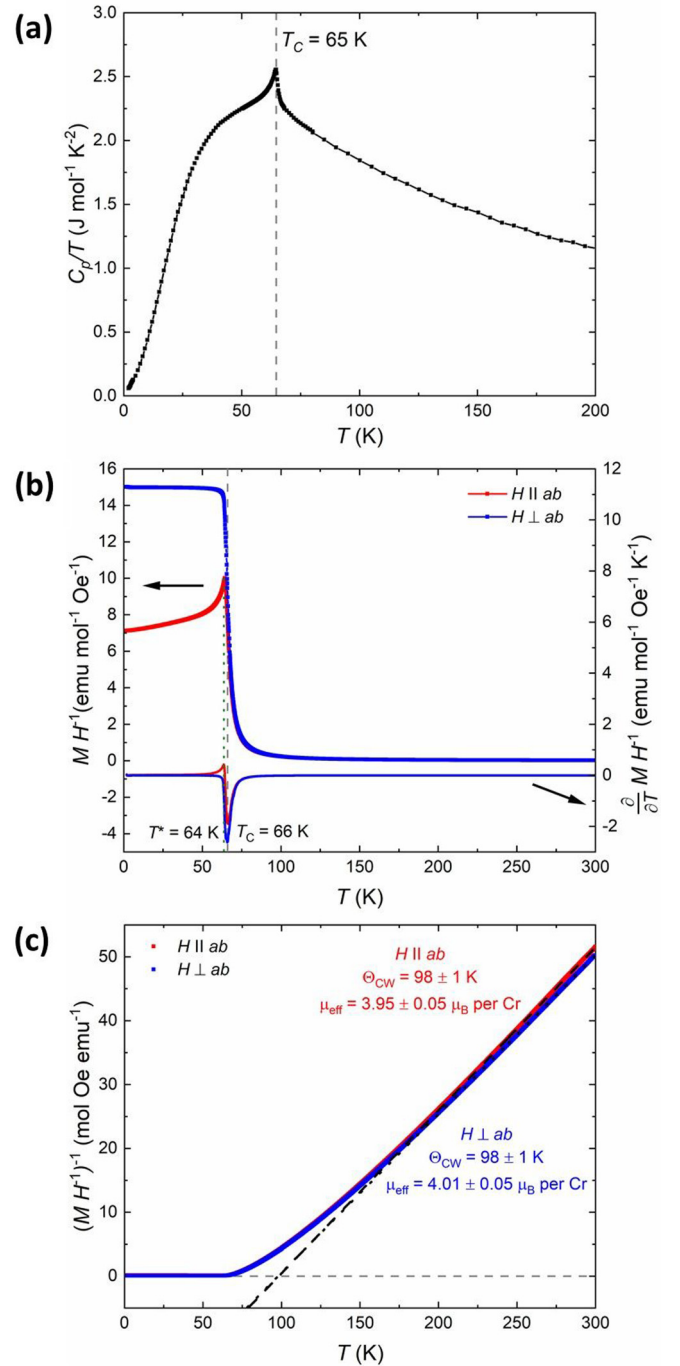


FIG. 3. (a) Zero-field specific heat divided by the temperature C_p/T of $\text{Cr}_2\text{Ge}_2\text{Te}_6$ as a function of temperature. (b) Temperature dependence of the normalized magnetization M/H and its first derivative at $H = 1$ kOe (field cooled). The grey dashed line indicates the Curie temperature T_C and the green dotted line indicates the temperature of the onset of the downturn T^* for $H \parallel ab$. (c) Inverse of the normalized magnetization $[(M/H)^{-1}]$ at $H = 1$ kOe. The black dashed and dotted lines show linear fits in the paramagnetic region ($200 \text{ K} < T < 300 \text{ K}$).

as shown in Eq. (1).

$$\chi(T) = \frac{\partial M}{\partial H} \approx \frac{M}{H}. \quad (1)$$

Consequently, in the paramagnetic state the normalized magnetization can be used for a Curie-Weiss analysis. From this analysis effective magnetic moments of $\mu_{\text{eff}} = 3.95 \pm 0.05 \mu_B/\text{Cr}$ for $H \parallel ab$ and $\mu_{\text{eff}} = 4.01 \pm 0.05 \mu_B/\text{Cr}$ for $H \perp ab$ are obtained, which are in good agreement with the expected magnetic moments for $\text{Cr}_2\text{Ge}_2\text{Te}_6$ using $g = 2.023(5)$ for $H \parallel ab$ and $g = 2.040(5)$ for $H \perp ab$ from our previous work [19]. Furthermore, our Curie-Weiss analysis yields a Curie-Weiss temperature of $\Theta_{\text{CW}} = 98 \pm 1 \text{ K}$ for both directions in good agreement with literature [18,33].

The positive Curie temperature indicates a dominant ferromagnetic coupling. In three-dimensional ferromagnets Θ_{CW} is generally found to be close to T_C . The difference between Θ_{CW} and T_C that is found for $\text{Cr}_2\text{Ge}_2\text{Te}_6$ is most likely an indication for the suppression of the magnetic order due to the two-dimensional nature of the compound and thus also of the magnetic interactions. This is in line with current results obtained from ferromagnetic resonance (FMR) and electron spin resonance (ESR) [19], which demonstrated the intrinsic two-dimensional nature of the magnetic interaction in $\text{Cr}_2\text{Ge}_2\text{Te}_6$.

Also, the temperature dependence of C_p/T in Fig. 3(a) shows characteristic features for the two-dimensional nature of the magnetism in $\text{Cr}_2\text{Ge}_2\text{Te}_6$: the Λ -shape peak is rather small with an estimated integral of approximately $\Delta S \approx 2 \text{ J/mol/K}$ compared to the expected value of the magnetic entropy change at a ferromagnetic ordering of a system with two $S = 3/2$ magnetic ions per unit cell, the latter being $S_{\text{mag}} = 2R\ln(4) = 23.05 \text{ J/mol/K}$. This reduced size of the peak at the magnetic transition is a common feature in quasi-2D magnets, which was for example already observed in the chromium trihalides CrX_3 with $X = \text{Cl}$ [34], Br [35], I [17], and in copper based quasi-2D molecular magnets such as copper pyrazine perchlorate $\text{Cu}(\text{Pz})_2(\text{ClO}_4)_2$ [36]. The missing entropy is most likely from magnetic fluctuations giving an important contribution to the specific heat even far above the magnetic ordering.

Figure 4 shows the isothermal magnetization of $\text{Cr}_2\text{Ge}_2\text{Te}_6$ at 1.8 K for $H \parallel ab$ and $H \perp ab$. The hysteresis of the magnetization as a function of field is negligible, showing the behavior expected for a soft ferromagnet. From the high-field region, a saturation magnetization of $M_S \approx 3\mu_B/\text{Cr}$ is obtained for both orientations. Thus, Cr^{3+} with $S = 3/2$ leads to an isotropic Landé factor of $g \approx 2$, which is in excellent agreement with recent results from FMR studies on this compound [19]. The saturation field is found as the x component of the intercept of two linear fits, one being a fit to the saturated regime at high fields and one being a fit of the unsaturated linear regime at low fields. While the saturation magnetization is isotropic, the saturation field is anisotropic and changes from $H_{\text{sat}} = 4.8 \text{ kOe}$ for $H \parallel ab$ to $H_{\text{sat}} = 2.3 \text{ kOe}$ for $H \perp ab$.

This anisotropic behavior in the isothermal magnetization is related to two different contributions: the intrinsic magnetic anisotropy of the material (magnetocrystalline anisotropy) and the shape anisotropy of the measured sample. As $\text{Cr}_2\text{Ge}_2\text{Te}_6$ grows as thin platelet crystals, the shape anisotropy must be explicitly taken into account. To evaluate the demagnetization factors the sample's dimensions were measured along its edges from which an equivalent

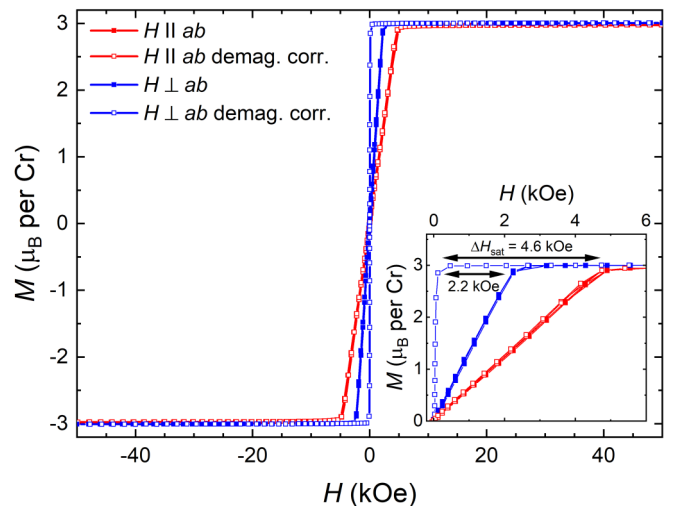


FIG. 4. Magnetization as function of field at 1.8 K for both crystallographic orientations (open symbols) and without (filled symbols) demagnetization field correction due to platelike sample shape (for details see text).

cuboid was constructed. The demagnetization factors of $N_x = N_y = 0.06$ and $N_z = 0.88$ were then calculated based on the equivalent-ellipsoid method [37,38].

As seen in Fig. 4, this correction strongly reduces the saturation field to 0.1 kOe for the orientation $H \perp ab$, while only a negligible shift to 4.7 kOe is obtained for $H \parallel ab$. The remaining anisotropy is purely originating from the magnetocrystalline anisotropy, showing that the magnetocrystalline easy axis is perpendicular to the crystallographic ab planes (or in turn parallel to the c direction).

Using the Stoner-Wolfarth model [39] a value for the magnetocrystalline anisotropy constant K_U can be estimated from the saturation regime in the isothermal magnetization curve. Within this model the magnetocrystalline anisotropy in the single domain state is related to the saturation field H_{sat} and the saturation moment M_S with μ_0 being the vacuum permeability:

$$\frac{2K_U}{M_S} = \mu_0 H_{\text{sat}}. \quad (2)$$

For $H \parallel ab$, where the anisotropy becomes maximal, this yields $K_U = 47 \pm 1 \text{ kJ/m}^3$ at 1.8 K. This value of K_U is in good agreement with K_U obtained previously by FMR on $\text{Cr}_2\text{Ge}_2\text{Te}_6$ [19].

In general, it can be expected that the anisotropic anomaly observed in temperature-dependent magnetization also manifests in the field dependence for $H \parallel ab$ (via a change of slope). Such a behavior was not resolved in our data at 1.8 K. This can be explained by the field dependence of T^* , which is investigated in detail in the following subsection.

B. Influence of external fields on the ground state

For $H \perp ab$ [Figs. 5(c) and 5(d)] the usual field dependence of ferromagnetic materials is observed. In our specific-heat studies the Λ -shape peak at T_C evolves into a broad maximum indicating that the magnetic transition becomes a crossover and this crossover is slightly shifted to higher

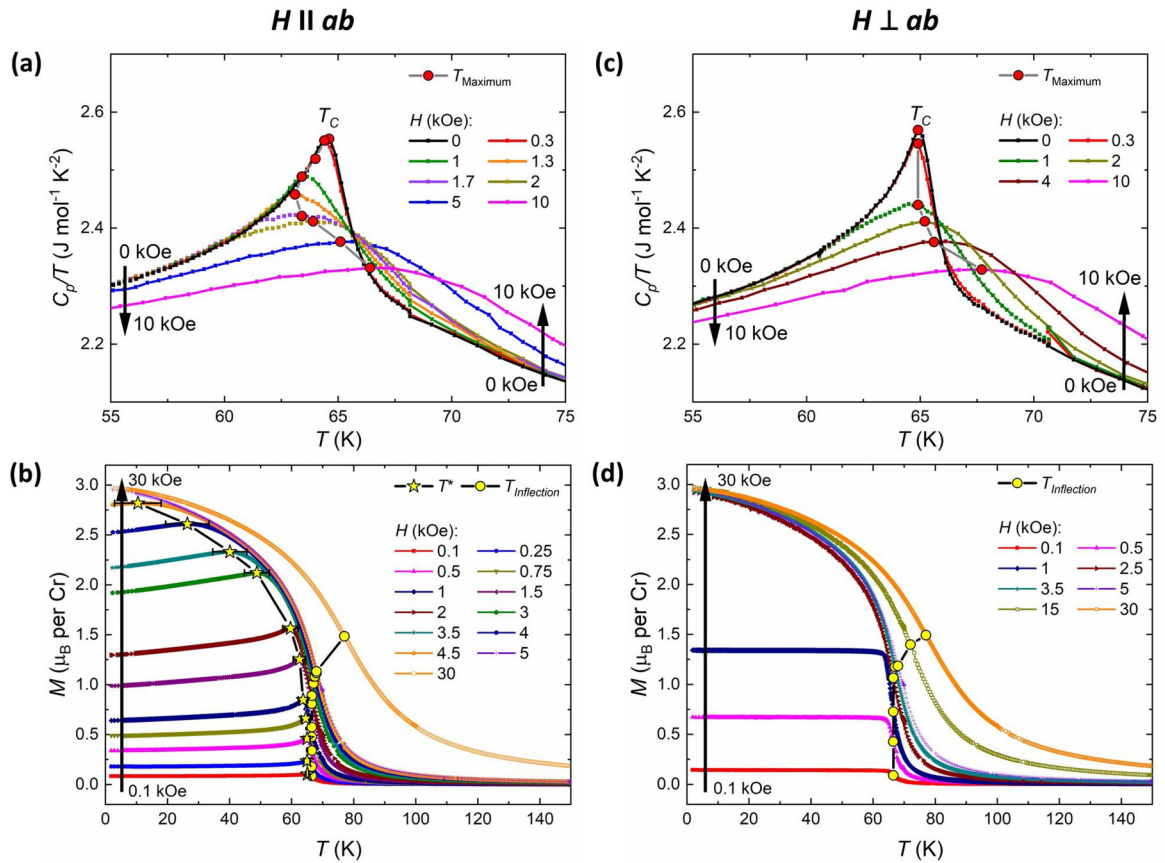


FIG. 5. Left: (a) C_p/T and (b) magnetization M as a function of temperature under different magnetic fields applied along the easy magnetization axis c . Right: (c) C_p/T and (d) magnetization M as a function of temperature under different magnetic fields applied in the hard magnetization plane ab . The maxima in C_p/T are marked with red dots in (a) and (c). The inflection points in $M(T)$ are marked with yellow dots in (b) and (d), while yellow stars in (b) indicate the maxima observed in $M(T)$ with $H \parallel ab$ corresponding to T^* .

temperature under magnetic fields. This is in agreement with the change seen in the temperature-dependent magnetization curve.

Overall, a different behavior is seen for $H \parallel ab$ [Figs. 5(a) and 5(b)]. While in the magnetization curves the ferromagnetic phase transition at T_C behaves in a similar way; for the lowest measured field of 0.1 kOe the downturn of the magnetization towards lower temperatures sets in just below the Curie temperature. This is indicated by a maximum in the magnetization curve at T^* [Fig. 5(b)]. By increasing the external field, T^* shifts towards lower temperatures. Additionally, upon increasing the external field, not just T^* shifts towards lower temperatures but also the maximum itself gets broadened and the downturn itself gets less pronounced. Finally at 5 kOe, which is close to the saturation field for the hard magnetization plane ab , no downturn is obtained anymore. Furthermore, comparing the temperature-dependent magnetization for $H \parallel ab$ and $H \perp ab$ at 5 kOe or higher fields, anisotropic magnetization is observed.

In comparison to the magnetization data, the specific heat only shows one clear phase transition for $H \parallel ab$, together with a change of the shift of the Λ -shaped peak position around 1.7 kOe [Fig. 5(a)]. By increasing the external field from zero up to 1.3 kOe the position of the maximum shifts towards lower temperatures. By increasing the external field further, the position of the maximum starts to shift towards

higher temperatures until an isotropic behavior is observed for fields of 5 kOe and higher. Furthermore, the progressive broadening of the maximum of C_p/T indicates an evolution of the nature of the transition from a second-order phase transition to a crossover.

Considering the strength of the downturn, seen in the temperature-dependent magnetization for $H \parallel ab$, an observable entropy change is expected to go along with its onset. Therefore a corresponding anomaly in $C_p/T(T)$ is expected. In the field range of 0 kOe and 1.3 kOe only one distinct signal is found in $C_p/T(T)$. However, in this field range T^* and T_C are close to each other (less than 3 K difference) and the Λ -shaped signal in the specific heat has a significant broadness. Therefore, it is not possible to state if only one anomaly is observed or if the signal contains actually two anomalies in this field range. However, as the signal in specific heat shifts towards lower temperatures, a dominant influence of the transition at T^* in this field regime can be expected.

While the crossover resulting from the PM-FM transition shifts towards higher temperatures as seen for $H \perp ab$ for both physical properties M and C_p , for $H \parallel ab$ and low fields the dominating T^* shifts towards lower temperatures and is illustrated via an anomaly in $C_p/T(T)$. For fields in the range of 1.7–5 kOe, however, the specific-heat measurements clearly show the absence of entropy changes at T^* but seems again to be sensitive to changes at T_C . This indicates that T^*

is a transition between two states with comparable magnetic entropy. At fields above 5 kOe the specific-heat behavior is isotropic for fields parallel and perpendicular to ab . This is in good agreement with the fields found for isotropic behavior in the temperature-dependent magnetization.

C. Low-field magnetic phase diagrams

For a better comparison between the peak position in specific heat and the significant temperatures from magnetization, the low-field magnetic phase diagrams for fields along the easy axis and the hard plane were constructed from our data. For fields along the easy axis [Fig. 6(b)], two phases are seen, i.e., a disordered paramagnetic phase (phase I) at high temperatures and a ferromagnetic ordered state with $M \parallel H$ (phase II) at lower temperatures. The transition temperatures from specific heat (peak position) and from magnetization (inflection point) are in good agreement within the range of the measurement uncertainties. In zero field the magnetization direction is supposed to be along the easy axis in the ferromagnetic state. Applying external fields parallel to the magnetic easy axis stabilizes this state for example against thermally activated magnetic fluctuations. Therefore, the observed behavior of phase II as function of field and temperature is well expected.

However, for $H \parallel ab$ an additional phase III is observed, as shown in Fig. 6(a). While for $H \perp ab$ the isomagnetization lines are parallel to the T axis until they deviate towards higher fields very close to T_C , for $H \parallel ab$, these lines first show a trend towards lower fields before they finally deviate towards high fields at elevated temperatures. These kinks are the fingerprints of the maximum seen in the temperature-dependent magnetization and are well followed by T^* . This allows us to not just define $T^*(H)$ but also $H^*(T)$ in this low-temperature/low-field regime. Whereas $T^*(H)$ corresponds to the signature of phase III in temperature-dependent magnetization, $H^*(T)$ corresponds to the same signature in field-dependent magnetization. Using the magnetic phase diagram for $H \parallel ab$ to estimate H^* (1.8 K) explains why no anomaly could be resolved in the corresponding isothermal magnetization in Fig. 4, as mentioned before. H^* (1.8 K) is estimated to be in the range of 4.5–4.7 kOe which is close to the saturation magnetization at this temperature. Consequently the slope of the $M(H)$ curve significantly changes in this field range and a separate anomaly corresponding to the signature of phase III is not resolved.

Besides the low-temperature/low-field regime (phase III) which is separated from the rest of the phase diagram by T^* , both phase diagrams resemble each other. This is best seen by comparing the course of the isomagnetization lines outside of phase III. Consequently, the magnetization in phases I and II is considered isotropic and the direction of the magnetization is parallel to the field for $T^* < T < T_C$ as seen for $H \perp ab$ (phase II).

Concluding from this behavior, the most likely scenario for the origin of the downturn in the magnetization curve for $H \parallel ab$ is a continuous reorientation of the magnetization direction as result of an interplay between the magnetocrystalline anisotropy, field, and temperature, as schematically shown in Fig. 7. The magnetocrystalline anisotropy favors a

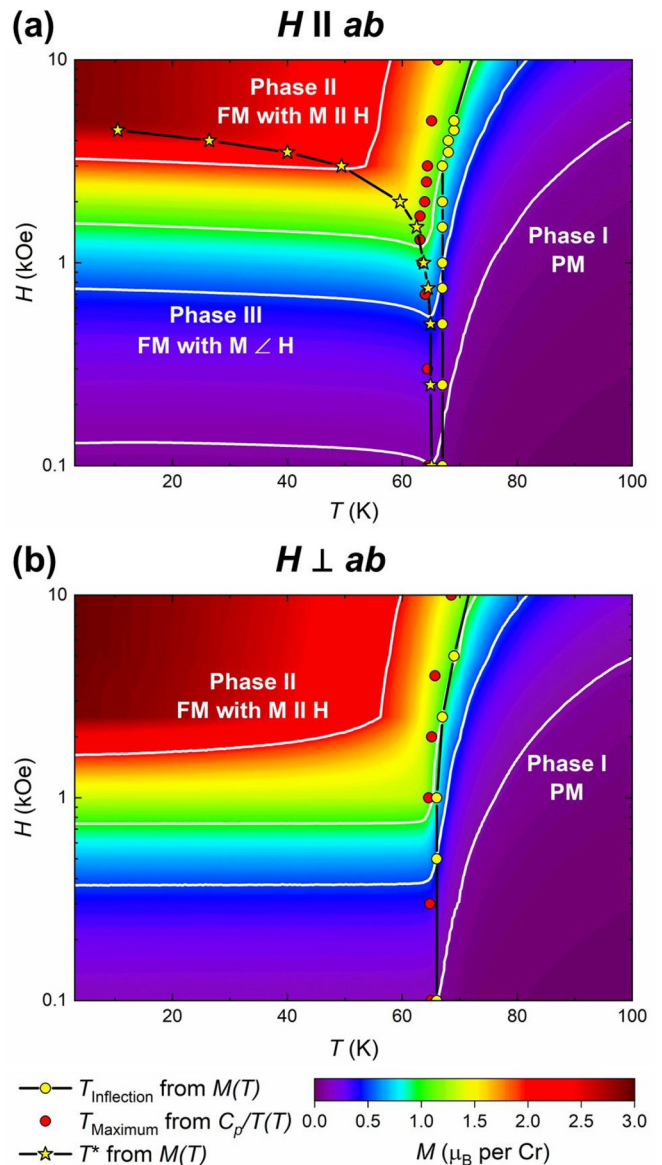


FIG. 6. Low-field magnetic phase diagram of $\text{Cr}_2\text{Ge}_2\text{Te}_6$ for (a) $H \parallel ab$ and (b) $H \perp ab$, where phase I is the paramagnetic state; phase II is the ferromagnetic state with $M \parallel H$; phase III only for $H \parallel ab$ is the ferromagnetic state with $M \perp H$ due to the interplay between $K_{U,\text{eff}}$, H , and T as schematically shown in Fig. 7. For both phase diagrams isomagnetization lines at 0.1, 0.5, 1, and $2 \mu_B$ are shown in white. The legend and the color scale at the bottom are applicable to both phase diagrams. Note that the magnetization shown in the phase diagrams is only the magnetization component parallel to H .

magnetization direction perpendicular to ab , while for $H \parallel ab$ the field wants to align the magnetization direction parallel to the field. Assuming an external field H_1 that is higher than H^* at a given temperature T_1 , the magnetization vector is aligned along the field direction (point 1 in Fig. 7). However, by reducing the external field to H_2 below H^* at the same temperature, a tilting of the magnetization vector away from the field direction will be achieved, i.e., a tilting towards the easy axis c in this case (point 2 in Fig. 7). This is due to

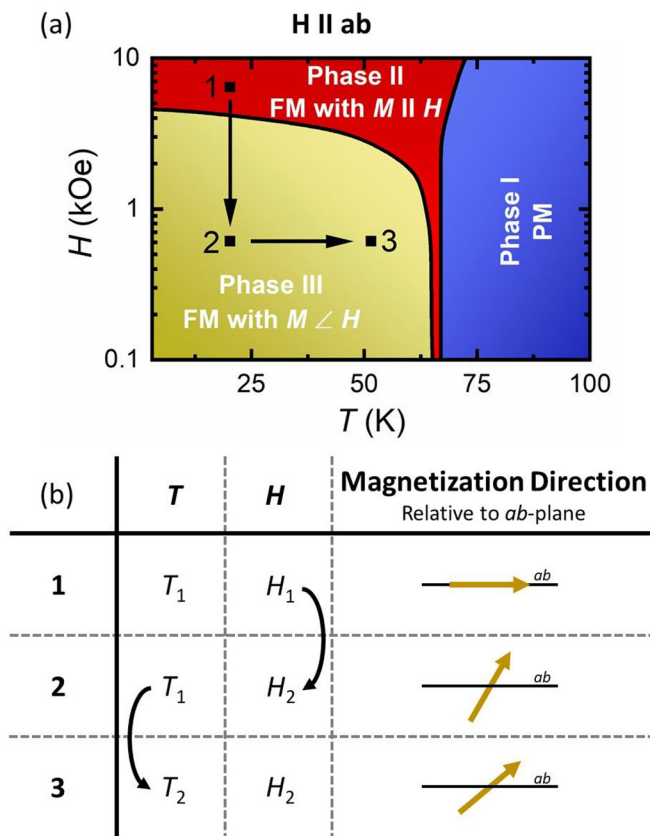


FIG. 7. (a) Schematic representation of the magnetic phase diagram of $\text{Cr}_2\text{Ge}_2\text{Te}_6$ for $H \parallel ab$ with the three magnetic phases as shown in Fig. 6(a) with three points indicated. These points are arbitrarily chosen, however, fulfill the following conditions: $T_1 < T_2 < T^*(100 \text{ Oe})$ and $H_1 > H^*(T_1) > H_2$. (b) Parameters T and H for every point together with the expected direction of the magnetization with respect to the ab plane. The black arrows in (a) correspond to the arrows in (b) and indicate which of the parameters T and H is changed. Please note that the arrow for the magnetization direction is supposed to only show the direction of the magnetization vector and not its absolute value.

the reduction of external field leading to similar energy scales of the magnetic field and the magnetocrystalline anisotropy. The tilting in turn leads to a reduction of the magnetization component parallel to the field ($\perp ab$ in this case).

In order to follow and describe this effect as function of temperature, a temperature-dependent magnetic anisotropy has to be taken into account. The magnetocrystalline anisotropy is caused by the underlying crystallographic lattice which is connected to the electronic spins via the spin-orbit coupling. As such, the magnetocrystalline anisotropy constant K_U is considered as a material constant which itself is independent of temperature and field.

However, many ferromagnets (e.g., Fe, Co, and Ni) exhibit a temperature dependence of the magnetocrystalline anisotropy constant on the macroscopic level. This observation can be understood based on the theory of Zener [40] who described the effect of temperature fluctuations on the anisotropy of the magnetization. According to his work, temperature leads to independent random fluctuations of local

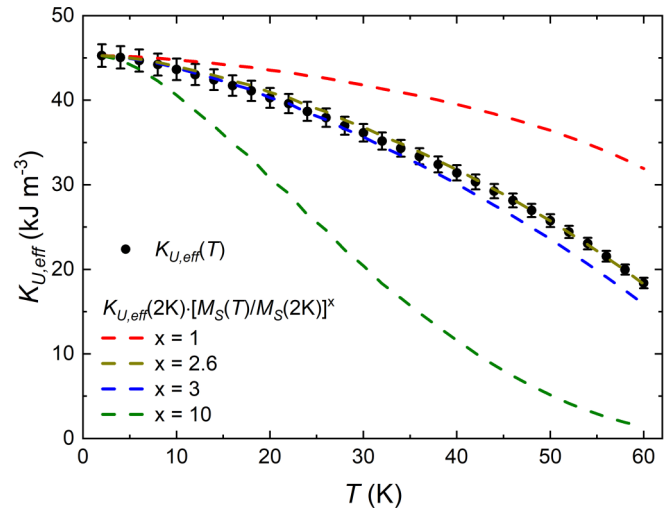


FIG. 8. Temperature evolution of the effective magnetic anisotropy constant $K_{U,\text{eff}}$ and the expected scaling of $K_{U,\text{eff}}$ according to the power-law behavior described in Eq. (3) using the exponents 1, 2.6, 3, and 10.

magnetization directions. In turn, this leads to an effective reduction of both macroscopic magnetization and anisotropy in the system. However, on a local scale the magnetization and magnetic anisotropy are temperature independent. To differentiate between the local temperature-independent and the global temperature-dependent magnetic anisotropy, $K_{U,\text{eff}}$ is introduced as an effective anisotropy constant which includes the effect of thermal fluctuations on a macroscopic scale and its interplay with the temperature-independent K_U . Based on Eq. (2), the temperature evolution of $K_{U,\text{eff}}$ was extracted from the magnetic phase diagram with fields parallel to the ab plane and is represented in Fig. 8. Details of how $K_{U,\text{eff}}$ was obtained are given in the Appendix.

As both the macroscopic magnetization and anisotropy are affected by thermal fluctuations, a proportionality between their evolution as a function of temperature can be expected. According to the theory by Callen and Callen [41], this proportionality can be expressed by a power-law behavior of

$$\frac{K_{U,\text{eff}}(T)}{K_U} = \left[\frac{M_S(T)}{M_S} \right]^{l(l+1)/2}. \quad (3)$$

Hereinafter, the approximations $K_U \approx K_{U,\text{eff}}(2 \text{ K})$ and $M_S \approx M_S(2 \text{ K})$ are used. In the case of uniaxial anisotropy $l = 2$ and an exponent of 3 are expected, while for cubic anisotropy $l = 4$ and an exponent of 10 are found.

Figure 8 shows the expected evolution of $K_{U,\text{eff}}(T)$ given by the power-law dependence of the saturation magnetization in Eq. (3) for exponents 1, 2.6, 3, and 10. The observed temperature dependence of $K_{U,\text{eff}}$ at low temperatures shows a good agreement with the Callen-Callen power law with an exponent of 3, which is expected for purely uniaxial anisotropy. However, at higher temperatures the exponent deviates from 3 towards 2.6. For the exponents 1 and 10 the power-law behavior does not follow $K_{U,\text{eff}}(T)$ and therefore direct scaling of the saturation magnetization with $K_{U,\text{eff}}$ as well as cubic anisotropy can be ruled out. The observed deviation of the exponent from a value of 3 may be attributed

to higher-order anisotropy contributions. Such contributions need to be considered even in some elemental ferromagnets like nickel [42] or Fe thin films [43,44]. One might speculate that materials with more complex crystal structures like $\text{Cr}_2\text{Ge}_2\text{Te}_6$ are more prone to exhibit higher-order anisotropic contributions. Another contribution that can influence the temperature dependence of the magnetocrystalline anisotropy is the surface anisotropy. This was demonstrated for example in NiFe_2O_4 nanomagnets [44]. However considering the surface-to-volume ratio, this effect should play only a secondary role in $\text{Cr}_2\text{Ge}_2\text{Te}_6$ bulk crystals compared to nanoparticles. Nevertheless, due to the thin platelet shape of the crystals the surface anisotropy can be expected to be slightly more dominant than in typical 3D crystals.

The agreement between the experimentally determined exponent with a value of 3 confirms that the magnetic anisotropy in $\text{Cr}_2\text{Ge}_2\text{Te}_6$ is uniaxial. Given the noncubic crystal structure and the good agreement of simulations and experimental values of the angular dependence of the resonance field in FMR using an uniaxial model in our previous work [19], this behavior is in accordance with previous work. Therefore, also the observed reduction of the magnetic anisotropy as function of temperature seems to be reliable.

It should be noted that Khan *et al.* also reported a temperature-dependent $K_{U,\text{eff}}$ for $\text{Cr}_2\text{Ge}_2\text{Te}_6$ which, however, scales with an exponent 4.71 [45]. They proposed that this deviation from the expected exponent of 3 is due to the role of spin-orbit coupling from Te atoms, which is not observed in our study. Furthermore, our analysis is very similar to Richter *et al.* on CrI_3 [20], who also do not see a significant role of spin-orbit coupling on the temperature-dependent $K_{U,\text{eff}}$ values in their compound.

Assuming a tilted magnetization vector due to the previously discussed interplay between the effective magnetic anisotropy and an external field perpendicular to the easy axis at T_1 (point 2 in Fig. 7), an increase in temperature to T_2 leads to a reduction of magnetic anisotropy. Therefore, the alignment along the magnetic easy axis becomes less favorable upon warming, which leads to a stronger tilting of the magnetization vector towards the ab plane and an increased experimentally determined ab component $\parallel H$ in this case (point 3 in Fig. 7).

Thus, T^* is the temperature at which the magnetization component along the easy axis becomes finite upon decreasing temperatures at a constant field in the ab plane. Vice versa, H^* is the field in the ab plane below which the easy axis magnetization component becomes finite at a constant temperature. A similar scenario was already proposed to explain a similar downturn of the transverse magnetization upon cooling below the Curie temperature in other ferromagnets: the structurally related quasi-two-dimensional ferromagnets CrX_3 ($X = \text{Br}, \text{I}$) [20] and the heavy Fermion ferromagnet URhGe [46].

For CrX_3 ($X = \text{Br}, \text{I}$) a similar analysis of $K_{U,\text{eff}}(T)$ was performed [20]. While the magnetocrystalline anisotropy constants of the chromium halides are larger than the one found for $\text{Cr}_2\text{Ge}_2\text{Te}_6$ (shown in Table I), their temperature dependence is also well described by exponents according to a uniaxial anisotropy. In the case of URhGe, the tilting of the magnetic moment in between the field direction and

TABLE I. Comparison between K_U for different (quasi-)2D honeycomb ferromagnets. Please note that for CrBr_3 and CrI_3 K_U was extracted from isothermal magnetization data at $T = 5$ K while for $\text{Cr}_2\text{Ge}_2\text{Te}_6$ data at $T = 1.8$ K was used.

Compound	K_U (kJ/m ³)	Reference
CrBr_3	86 (± 6)	Richter <i>et al.</i> [20]
CrI_3	301 (± 50)	Richter <i>et al.</i> [20]
$\text{Cr}_2\text{Ge}_2\text{Te}_6$	47 (± 1)	this work

the easy magnetization axis was directly observed by neutron diffraction [47] and NMR [48]. For URhGe a Ginzburg-Landau description of the anisotropic ferromagnet proposed by Mineev [49] reproduced the downturn of the magnetization and could possibly also be a promising model for a simple description of the low-field magnetic properties of $\text{Cr}_2\text{Ge}_2\text{Te}_6$. Another material that exhibits a similar anomaly in the temperature-dependent magnetization is PbMnBO_4 as reported by Pankrats *et al.* [50], where a similar interplay between the temperature dependence of the magnetic anisotropy and the before mentioned anomaly based on the temperature dependence of the anisotropy fields was concluded.

IV. SUMMARY

In summary, detailed magnetic and thermodynamic measurements were performed on high quality $\text{Cr}_2\text{Ge}_2\text{Te}_6$ single crystals. Analysis of the low-field data shows an interesting interplay of K_U , applied magnetic field, and temperature. $\text{Cr}_2\text{Ge}_2\text{Te}_6$ is a soft ferromagnet with a Curie temperature $T_C = 65$ K. An effective moment $\mu_{\text{eff}} \approx 4\mu_B/\text{Cr}$ and an isotropic saturation moment $M_S = 3\mu_B/\text{Cr}$ were found, both being in good agreement with the values expected for Cr^{3+} . Furthermore, the isotropic saturation magnetization hints towards an isotropic Landé factor $g \approx 2$. The difference between $\Theta_{\text{CW}} = 95$ K and T_C as well as the shape of the temperature-dependent specific heat indicate low-dimensional magnetic correlations well above the magnetic ordering temperature. The easy-axis nature of the magnetic properties perpendicular to the structural layers in the ab plane is confirmed and a magnetocrystalline anisotropy constant $K_U = 47 \pm 1$ kJ/m³ is obtained using the Stoner-Wolfarth model [39].

The field and temperature dependence of the magnetization was studied in detail for fields parallel and perpendicular to the hard magnetic plane ab up to fields of 30 kOe. Corresponding magnetic phase diagrams were constructed. The field and temperature dependence for fields along the easy axis $\parallel c$ show the typical behavior of a ferromagnet. However, for fields applied in the hard plane ab below a temperature $T^* < T_C$ a downturn towards lower temperatures is found in magnetization curves below the saturation field $H_{\text{sat},ab} \approx 5$ kOe. The origin of this anisotropic anomaly is discussed in terms of an interplay between the effective magnetic anisotropy $K_{U,\text{eff}}$, temperature, and the applied magnetic field. In this scenario, the magnetization direction continuously changes between a field-parallel configuration above T^* to a tilted direction with a magnetization component perpendicular to H . Thus, the temperature T^* can be understood as the temperature where

the magnetization component perpendicular to the ab plane changes from zero to finite.

To investigate the validity of the temperature dependence of the magnetic anisotropy, values for $K_{U,\text{eff}}$ were extracted at different temperatures from the magnetic phase diagram for $H \parallel ab$ and compared with a power-law scaling of the temperature-dependent saturation magnetization according to Callen and Callen [41]. The observed power-law behavior fits reasonably well for uniaxial anisotropy models.

A similar anisotropic anomaly was observed for CrX_3 (with $X = \text{Br}, \text{I}$) and also discussed in terms of interplay between $K_{U,\text{eff}}$ and temperature [20]. All these compounds share the same magnetic ion and easy axis $\parallel c$ ferromagnetic ordering together with a similar 2D honeycomb lattice. Thus, the magnetocrystalline anisotropies in these systems are similar, although the magnetocrystalline anisotropy constant K_U shows significant differences in its absolute value for the mentioned compounds. This hints towards a universality of this interplay in quasi-two-dimensional ferromagnetic materials. Furthermore, the observed anomaly in the temperature dependence of the magnetization can be considered as a fingerprint of this interplay.

Besides all similarities, these compounds also show influential differences in the nature of their magnetism, for example in the type of magnetic coupling. The TMTCs ($\text{Cr}_2\text{Ge}_2\text{Te}_6$ [18] and $\text{Cr}_2\text{Si}_2\text{Te}_6$ [51]) exhibit 2D Ising-like behavior while CrX_3 ($X = \text{Br}$ [52], I [53]) display a more 3D Ising-like coupling, according to investigations of the critical behavior of these compounds due to interlayer interactions present at least in the bulk state. Taken the 2D nature and the high Curie temperature of $\text{Cr}_2\text{Ge}_2\text{Te}_6$, this compound could be a highly promising low-dimensional ferromagnet to gain further insight into low-dimensional ferromagnetism in general and for use in ferromagnetic heterostructures.

ACKNOWLEDGMENTS

S.S. acknowledges financial support from GRK-1621 Graduate Academy (Project No. 129760637) of the Deutsche Forschungsgemeinschaft (DFG). G.B. acknowledges financial support from the European Union's Horizon 2020 research

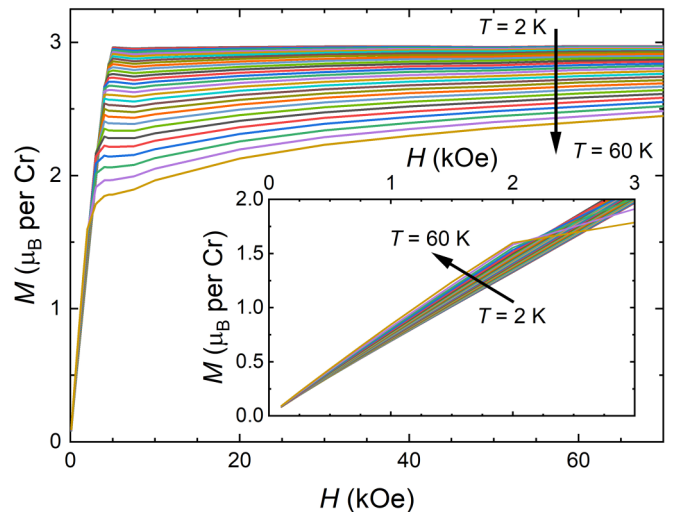


FIG. 9. Isothermal magnetization for $H \parallel ab$ in a range from 2 to 60 K in 2-K steps extracted from the corresponding magnetic phase diagram. The inset shows the evolution of the linear behavior at low fields as function of temperature in more detail.

and innovation program under the Marie Skłodowska-Curie Grant Agreement No. 796048. S.A. acknowledges financial support from DFG via Grant No. AS 523/4-1. A.U.B.W. and B.B. acknowledge financial support from the DFG through SFB 1143 (Project No. 247310070).

APPENDIX

Extraction of $K_{U,\text{eff}}$ as function of temperature

To obtain the temperature dependence of $K_{U,\text{eff}}$, isothermal magnetization curves were extracted from the magnetic phase diagram for $H \parallel ab$ in the range of 2–60 K (shown in Fig. 9). The saturation magnetization and the saturation field at each temperature were obtained from the intersection of two linear regressions of the low-field (0–2 kOe) and the high-field region (30–70 kOe), respectively. From these values $K_{U,\text{eff}}$ was obtained for each temperature based on Eq. (2).

- [1] K. S. Novoselov, *Science* **306**, 666 (2004).
- [2] K. F. Mak, C. Lee, J. Hone, J. Shan, and T. F. Heinz, *Phys. Rev. Lett.* **105**, 136805 (2010).
- [3] A. Splendiani, L. Sun, Y. Zhang, T. Li, J. Kim, C.-Y. Chim, G. Galli, and F. Wang, *Nano Lett.* **10**, 1271 (2010).
- [4] X. Xi, L. Zhao, Z. Wang, H. Berger, L. Forró, J. Shan, and K. F. Mak, *Nat. Nanotechnol.* **10**, 765 (2015).
- [5] S. Kolekar, M. Bonilla, Y. Ma, H. C. Diaz, and M. Batzill, *2D Mater.* **5**, 015006 (2017).
- [6] A. W. Tsen, B. Hunt, Y. D. Kim, Z. J. Yuan, S. Jia, R. J. Cava, J. Hone, P. Kim, C. R. Dean, and A. N. Pasupathy, *Nat. Phys.* **12**, 208 (2015).
- [7] A.-S. Pawlik, S. Aswartham, I. Morozov, M. Knupfer, B. Büchner, D. V. Efremov, and A. Koitzsch, *Phys. Rev. Mater.* **2**, 104004 (2018).
- [8] L. D. Alegria, H. Ji, N. Yao, J. J. Clarke, R. J. Cava, and J. R. Petta, *Appl. Phys. Lett.* **105**, 053512 (2014).
- [9] K. S. Novoselov, A. Mishchenko, A. Carvalho, and A. H. C. Neto, *Science* **353**, aac9439 (2016).
- [10] A. K. Geim and I. V. Grigorieva, *Nature (London)* **499**, 419 (2013).
- [11] C. Gong, L. Li, Z. Li, H. Ji, A. Stern, Y. Xia, T. Cao, W. Bao, C. Wang, Y. Wang, Z. Q. Qiu, R. J. Cava, S. G. Louie, J. Xia, and X. Zhang, *Nature (London)* **546**, 265 (2017).
- [12] B. Huang, G. Clark, E. Navarro-Moratalla, D. R. Klein, R. Cheng, K. L. Seyler, D. Zhong, E. Schmidgall, M. A. McGuire, D. H. Cobden, W. Yao, D. Xiao, P. Jarillo-Herrero, and X. Xu, *Nature (London)* **546**, 270 (2017).
- [13] M.-W. Lin, H. L. Zhuang, J. Yan, T. Z. Ward, A. A. Puretzy, C. M. Rouleau, Z. Gai, L. Liang, V. Meunier, B. G. Sumpter,

- P. Ganesh, P. R. C. Kent, D. B. Geohegan, D. G. Mandrus, and K. Xiao, *J. Mater. Chem. C* **4**, 315 (2016).
- [14] C. Xu, J. Feng, H. Xiang, and L. Bellaiche, *npj Comput. Mater.* **4**, 57 (2018).
- [15] M. Bonilla, S. Kolekar, Y. Ma, H. C. Diaz, V. Kalappattil, R. Das, T. Eggers, H. R. Gutierrez, M.-H. Phan, and M. Batzill, *Nat. Nanotechnol.* **13**, 289 (2018).
- [16] X. Zhang, Y. Zhao, Q. Song, S. Jia, J. Shi, and W. Han, *Jpn. J. Appl. Phys.* **55**, 033001 (2016).
- [17] M. A. McGuire, H. Dixit, V. R. Cooper, and B. C. Sales, *Chem. Mater.* **27**, 612 (2015).
- [18] Y. Liu and C. Petrovic, *Phys. Rev. B* **96**, 054406 (2017).
- [19] J. Zeisner, A. Alfonsov, S. Selter, S. Aswartham, M. P. Ghimire, M. Richter, J. van den Brink, B. Büchner, and V. Kataev, *Phys. Rev. B* **99**, 165109 (2019).
- [20] N. Richter, D. Weber, F. Martin, N. Singh, U. Schwingenschlögl, B. V. Lotsch, and M. Kläui, *Phys. Rev. Mater.* **2**, 024004 (2018).
- [21] N. D. Mermin and H. Wagner, *Phys. Rev. Lett.* **17**, 1133 (1966).
- [22] C. Gong and X. Zhang, *Science* **363**, eaav4450 (2019).
- [23] S. Blundell, *Magnetism In Condensed Matter*, 2nd ed. (Oxford University Press, New York, 2000).
- [24] V. Carteaux, D. Brunet, G. Ouvrard, and G. Andre, *J. Phys.: Condens. Matter* **7**, 69 (1995).
- [25] R. Brec, in *Intercalation in Layered Materials* (Springer, New York, 1986), pp. 93–124.
- [26] E. Sandre, V. Carteaux, A. Marie, and G. Ouvrard, *J. Alloys Compd.* **204**, 145 (1994).
- [27] A. R. Wildes, V. Simonet, E. Ressouche, G. J. McIntyre, M. Avdeev, E. Suard, S. A. J. Kimber, D. Lançon, G. Pepe, B. Moubaraki, and T. J. Hicks, *Phys. Rev. B* **92**, 224408 (2015).
- [28] G. Ouvrard, R. Brec, and J. Rouxel, *Mater. Res. Bull.* **20**, 1181 (1985).
- [29] A. Mishra and S. B. Lee, *Sci. Rep.* **8**, 799 (2018).
- [30] H. Ji, R. A. Stokes, L. D. Alegria, E. C. Blomberg, M. A. Tanatar, A. Reijnders, L. M. Schoop, T. Liang, R. Prozorov, K. S. Burch, N. P. Ong, J. R. Petta, and R. J. Cava, *J. Appl. Phys.* **114**, 114907 (2013).
- [31] Q. Desgin, Accuracy of the Reported Moment: Sample Shape Effects - SQUID VSM Application Note 1500-015, Technical Report, Quantum Design, 2010, <https://www.qdusa.com/siteDocs/appNotes/1500-015.pdf>.
- [32] L. D. Casto, A. J. Clune, M. O. Yokosuk, J. L. Musfeldt, T. J. Williams, H. L. Zhuang, M.-W. Lin, K. Xiao, R. G. Hennig, B. C. Sales, J.-Q. Yan, and D. Mandrus, *APL Mater.* **3**, 041515 (2015).
- [33] G. T. Lin, H. L. Zhuang, X. Luo, B. J. Liu, F. C. Chen, J. Yan, Y. Sun, J. Zhou, W. J. Lu, P. Tong, Z. G. Sheng, Z. Qu, W. H. Song, X. B. Zhu, and Y. P. Sun, *Phys. Rev. B* **95**, 245212 (2017).
- [34] M. A. McGuire, G. Clark, S. KC, W. M. Chance, G. E. Jellison, V. R. Cooper, X. Xu, and B. C. Sales, *Phys. Rev. Mater.* **1**, 014001 (2017).
- [35] L. D. Jennings and W. N. Hansen, *Phys. Rev.* **139**, A1694 (1965).
- [36] T. Lancaster, S. J. Blundell, M. L. Brooks, P. J. Baker, F. L. Pratt, J. L. Manson, M. M. Conner, F. Xiao, C. P. Landee, F. A. Chaves, S. Soriano, M. A. Novak, T. P. Papageorgiou, A. D. Bianchi, T. Herrmannsdörfer, J. Wosnitzer, and J. A. Schlueter, *Phys. Rev. B* **75**, 094421 (2007).
- [37] J. A. Osborn, *Phys. Rev.* **67**, 351 (1945).
- [38] D. C. Cronemeyer, *J. Appl. Phys.* **70**, 2911 (1991).
- [39] E. C. Stoner and E. P. Wohlfarth, *Philos. Trans. R. Soc. A* **240**, 599 (1948).
- [40] C. Zener, *Phys. Rev.* **96**, 1335 (1954).
- [41] H. Callen and E. Callen, *J. Phys. Chem. Solids* **27**, 1271 (1966).
- [42] W. J. Carr, *Phys. Rev.* **109**, 1971 (1958).
- [43] D. P. Pappas, *J. Vacuum Sci. Technol. B* **14**, 3203 (1996).
- [44] B. K. Chatterjee, C. K. Ghosh, and K. K. Chattopadhyay, *J. Appl. Phys.* **116**, 153904 (2014).
- [45] S. Khan, C. W. Zollitsch, D. M. Arroo, H. Cheng, I. Verzhbitskiy, A. Sud, Y. P. Feng, G. Eda, and H. Kurebayashi, *Phys. Rev. B* **100**, 134437 (2019).
- [46] F. Hardy, D. Aoki, C. Meingast, P. Schweiss, P. Burger, H. v. Löhneysen, and J. Flouquet, *Phys. Rev. B* **83**, 195107 (2011).
- [47] F. Lévy, I. Sheikin, B. Grenier, and A. D. Huxley, *Science* **309**, 1343 (2005).
- [48] H. Kotegawa, K. Fukumoto, T. Toyama, H. Tou, H. Harima, A. Harada, Y. Kitaoka, Y. Haga, E. Yamamoto, Y. Ōnuki, K. M. Itoh, and E. E. Haller, *J. Phys. Soc. Jpn.* **84**, 054710 (2015).
- [49] V. P. Mineev, *Phys. Rev. B* **83**, 064515 (2011).
- [50] A. Pankrats, K. Sablina, M. Eremin, A. Balaev, M. Kolkov, V. Tugarinov, and A. Bovina, *J. Magn. Magn. Mater.* **414**, 82 (2016).
- [51] B. Liu, Y. Zou, L. Zhang, S. Zhou, Z. Wang, W. Wang, Z. Qu, and Y. Zhang, *Sci. Rep.* **6**, 33873 (2016).
- [52] J. T. Ho and J. D. Litster, *J. Appl. Phys.* **40**, 1270 (1969).
- [53] Y. Liu and C. Petrovic, *Phys. Rev. B* **97**, 014420 (2018).